Effect of impurities argon and moisture additives on laser ignition of n-decane/air mixtures

Nabil Mokrani[1], Steve Rudz[1,*] and Philippe Gillard[1]

[1]Laboratoire PRISME, Univ. Orléans, INSA-CVL, EA 4229, F-18020 Bourges, France.

[*]Corresponding author: Steve Rudz, Laboratoire PRISME, IUT de Bourges 63, Avenue de Lattre de Tassigny 18020 Bourges, France.

E-mail: steve.rudz@univ-orleans.fr

Phone: +33248238223

Abstract

Ignition using laser breakdown of n-decane/air mixtures was investigated to highlight the influence of Argon, moisture, concentration and focal length on laser ignition probabilities. The effect of fuel impurities on Minimum Ignition Energy (MIE) was also investigated. Characterization was performed using a Q-switched Nd-YAG laser (1064nm) with a cylindrical vessel at a fixed temperature of 347 K and atmospheric pressure. The ignition probabilities obtained depended on the concentration of argon and water present in the combustion mixture. Results showed that Ar and H_2O play a significant role in the breakdown process inducing ignition. MIE was determined for pure n-decane 99% and compared with the results of an impure n-decane 94% tested in a previous study. Finally Ignition Delay Time (*IDT*) measured by recording photodiode signals and spectroscopic analysis was used to characterize ignition of the studied reactive mixtures as a function of different equivalence ratios.

Keywords: *Breakdown; n-decane; Laser; Probabilities; Moisture and argon effect; MIE; impurity; Ignition delay; Spectroscopy*

1. Introduction

Due to economic and environmental constraints, a further reduction in the fuel consumption and the exhaust emissions of several engines is required (Chehroudi, 2004). At the moment, direct injection fuel engines show the highest potential for such reductions. Unfortunately, conventional spark plug ignition has a major disadvantage with respect to modern spray-guided combustion processes since the ignition location cannot be chosen optimally, and it is not possible to ignite inside the fuel spray (Hatwar & Verma, 2012). Moreover leaner mixtures cannot be burned and often higher turbulence levels are required (Cardin et al., 2013a). These difficulties can be overcome by using a laser breakdown which allows a more flexible choice of

the ignition location inside the combustion chamber and offers the possibility to ignite even inside spray with leaner, high ratio mixtures for different performances (Hatwar & Verma, 2012). Added to this, higher turbulence levels are not required for this system (Cardin et al., 2013b; Griffiths et al., 2015a). However, despite all the these advantages, laser ignition is not yet fully understood, either from the combustion or the plasma breakdown point of view (Mokrani et al., 2015). This new system which uses an intense unidirectional beam of light, with short powerful pulse is able to produce breakdown in air/fuel gas at intensities in the range of 10^{10}- 10^{11}W/cm^2 (Hatwar & Verma, 2012). At such intensities, gas molecules are dissociated and ionized within the focal spot of the laser beam and a small volume of plasma is generated. This phenomenon has also been numerically studied by several authors (Thiele et al., 2000; Morsy & Chung, 2002; Jiping et al., 2015). Once the plasma has been generated, it is heated by the incoming beam of photons, generating a strong shock wave. The plasma can be used to ignite diverse fuel-gas mixtures (Jain & Kozola, 2001; Phuoc, 1999; McNeill, 2005; Phuoc, 2006). The laser spark begins with the multi-photon ionization of a few gas molecules which release electrons that readily absorb more photons via the inverse Bremsstrahlung process to increase their kinetic energy (Pakter, 1998). The electrons thus released collide with other molecules and ionize them, leading to an electron avalanche, and breakdown of the gas (Starikovskiy & Aleksandrov, 2013).

The investigated fuel in this study is the n-decane because it is a surrogate of the kerosene used in aeronautical propulsion. The burning of this fuel leads to different amounts of pollutants due to operating conditions (for example take-off, flying and landing), and also purity of fuel and air. Several works have been conducted to achieve a greener combustion. From the late 70's Jones (1978)

pointed out that impurities contained in the used fuel are responsible of the formation of CO, SO_x, THC and NO_x. At the beginning of this century Lilley (2003) has highlighted that operating at low temperatures increase the amount of produced THC and CO while at high temperature it is the amount of NO_x which rise. To achieve low temperatures one can resize the combustion chamber (Jones, 1978) or add demineralized water (Boretti, 2013) or Argon gas (Karthieya Sharma, 2014). Those four last references underlined separately that both impurities contained in fuel and air play a significant role during the combustion process. The experimental work undertaken in this paper is the study on the ignition properties of n-decane/air mixtures for several air compositions (synthetic air $0.2O_2 + 0.8N_2$ with or without add of Argon or moisture) and two purity for n-decane (94 and 99%).The present work first reports experimental ignition probabilities in order to demonstrate the effects of argon, moisture and impurities contained in the n-decane fuel. Measurements of Minimum Ignition Energy (MIE) were performed to highlight the action of impurities by comparing an impure n-decane (94%) with a pure n-decane (99%). Secondly, ignition delay time was measured by analyzing spectra and photodiode signals for an n-decane/air mixture at different equivalence ratios with 99% of purity for the n-decane. The MIE of the n-decane/air mixtures was measured using an experimental laser-induced spark ignition system previously developed in Tihay et al. (2012) and upgraded in Rudz et al. (2014) for absorbed energy measurements.

The article is structured as follows. Sections 2 and 3 present the experimental setup and experimental method and procedures used to determine the ignition probabilities, Minimum Ignition Energy (MIE) and Ignition Delay Time (IDT) of the mixture.

Section 4 presents the results and discussion. The last section draws some conclusions from this study.

2. Experimental setup

In this work, the LIQUIM (Laser Ignition in QUIescent Mixtures) apparatus equipped with a spectrometer was used to perform Ignition Delay measurements. A sketch of the setup is given in Figure 1. Key aspects of the apparatus are briefly recalled here; for a more detailed overview the reader is referred to Rudz et al. (2014), Strozzi et al. (2014) and Tihay et al. (2012). The combustion chamber is a cylindrical vessel of 10^{-3} m^3 (*L = 0.2 m and D = 0.8 m*) filled with synthetic air (*80% N_2, 20% O_2, CO2 <1 ppm, CO<1 ppm, H2O < 3 ppm, CnHm < 0.1 ppm*). The first liquid n-decane was provided by ALFA AESAR (*reference A14732.AP*) with a *99 %* degree of purity, and the second n-decane reference is provided by MERCK (*reference 8.20383.1000*) with a *94 %* degree of purity.

The reactive mixtures are ignited by means of a laser beam provided by a Q-switched Nd:YAG laser (*Quantel Brilliant*) operating at *1064 nm*. The laser beam enters and exits the vessel through two antireflection coated windows. The incident energy coming from the laser and transmitted through the mixture is measured by two Ophir Nova energy meters (see Figure 2). The incident energy (E_{inc}) is calculated thanks to the first energy meter located behind the beam splitter, see Eq. 1:

$$E_{inc} = E_{ref}\left[\frac{(1-\rho)}{\rho}\right] \qquad (1)$$

with (ρ) the coefficient of the beam splitter.

Figure 1 approximately here

Then the energy absorbed (E_{abs}) by the plasma is calculated knowing the transmission coefficient (τ) of the two antireflection coated windows and the focal length, the measurement of this energy (E_{abs}) is given by Eq. 2:

$$E_{abs} = \tau E_{inc} - E_{trans} \quad (2)$$

The two coefficients (ρ) and (τ) depend on the atmospheric conditions. They were therefore calibrated every day and for every change in the energy of the laser source. Slight variations were observed for both $\rho \approx 0.016 \pm 0.001$ and $\tau \approx 0.96 \pm 0.02$. During the calibration process, the reactor was under vacuum.

Figure 2 approximately here

During experiments the ignition delay was measured with an infrared detector sensor (*H250 SIEMENS SF*). The collected signal was amplified before being recorded by a digital oscilloscope. This was used for two reasons: firstly it has a short response time of *10 ns* which is largely consistent with the time scales of the studied phenomena and secondly it has a maximum sensitivity in the near infrared $\lambda_{max} = 850$ *nm* with a sensitivity ranging from *400 nm* to *1100 nm*. The detector was used to detect the spark and the flame emission light from the laser for each ignition trial.

An Ocean Optics *HR2000+ES* spectrometer was used to track the induced spark and the flame light emissions with a wavelength resolution of *0.5 nm* and an acquisition frequency of 500 *Hz*. The bandwidth ranged from 189 nm to 1100 nm.

3. Experimental procedures

Before injecting the fuel the chamber was placed under vacuum ($P \approx 0.003$ mbar). Then the liquid fuel was directly injected into the combustion chamber through a septum using a micrometric syringe. Synthetic air was then admitted with a flow rate of approximately 2 L/min. The equivalence ratio was calculated from the mass of liquid n-decane and the total pressure P was 1 bar. Pressure was checked from the fuel

vapour pressure value when the n-decane had been fully vaporized. The combustion chamber and the air intake line were heated at T = 347 K. In order to remove residual combustion products and residual moisture, the chamber was filled with synthetic air and placed under vacuum three times between consecutive reactive experiments. The walls and windows of the chamber were periodically cleaned. Occurrence of laser breakdown and ignition were detected by the observation of light emission with the naked eye and by using photodiodes and emission spectroscopy.

The relative probability of breakdown or ignition was defined as the ratio of positive trials and the number of shots obtained for a given value of incident energy. For breakdown, a positive test corresponded to the formation of plasma, which was characterized by a flash of light and a sharp acoustic sound. For ignition, a positive test involved the formation of a flame front, an increase of pressure inside the chamber and combustion of the mixture. The reactive mixture was obtained from synthetic air and from liquid n-decane with a 94 % degree of purity (for the first experiments) to highlight the effect of Argon and moisture. The experiment design is given in Table 1. The incident energy E_{inc} ranged from 10 to 60 mJ with a step of 10 mJ for a total of *1080* shots using one equivalence ratio of ϕ=1.1.

Table 1 approximately here

A second set of experiments was carried out with pure n-decane (99% degree of purity) to investigate the effect of impurities. Measurements and analysis of the photodiode signals and emission spectra from the breakdowns and the combustion were also performed. Six equivalence ratios (*0.65, 0.9, 1.1, 1.3, 1.6* and *2*) and 8 incident energies of the laser source (from *10* to *80 mJ* with a *10 mJ* step) were investigated, for a total of *2400* shots in this second study.

4. Results and discussion

4.1. Statistical study

4.1.1. Effect of Argon and Moisture

Argon and moisture are known to be factors that affect thermal efficiency and gas emission. Several studies showed the influence of additives and diluents on releases of greenhouse gas. For example, a comparison conducted by He et al. (2015) for CO_2, N_2 and Ar showed that CO_2 is the most effective reducing NO_x and CO emission followed by N_2. However, both CO_2 and N_2 dilution weakened the thermal efficiency while Ar dilution improved it. Many effects of Ar are also discussed by Li et al. (2015) in the case of natural gas engines. Experimental work by Zhang et al. (2015) into the effects of two diluents, i.e., argon and nitrogen, on a dimethyl ether (DME)–air mixture showed that, the explosion parameters of fuel-lean and fuel-rich mixtures exhibit different behaviours. The effect of moisture was investigated by Nikolaou et al. (2013) who reported some effect of H_2O using a reduced kinetic mechanism. It therefore appeared essential in the present study to look at the effect of the two additives Argon and moisture on ignition properties.

The first step of our study aimed to highlight the influence of argon and moisture on the ignition probability by using statistical analysis. A decane (94%)-air mixture with an equivalence ratio of ϕ=1.1 was used and various compositions, depicted in Table 1, were investigated. The results are reported on Figure 3.

Figure 3 approximately here

These experiments showed that a combination of additives (Ar, H_2O) has a significant effect on the probability of ignition compared to experiments without any additives. With 1% of Argon, which is close to the composition of ambient air, and without

humidity, this additive plays a role of ignition catalyst at low incident energies, and acts as an ignition inhibitor at 30 and 40 mJ incident energies. Results show the behaviour of Argon on the excitation energy, because in some cases Argon can be used as a photon pumping source and as a reception well to stabilize the plasma at high energies. The low ignition zone ranges from 30 to 40 mJ for Argon.

For moisture (30 mbar H_2O) ignition frequencies increased as a function of incident energy with a moderate catalyst effect compared with reference case. At high temperature the polyatomic molecule of H_2O can often be used as an oxidizing source that increases the concentration of oxygen (O_2). The combined configuration of (30 mbar H_2O and 1 % Ar) makes the mixture very sensitive and easy to ignite, no doubt due to the combined effect of Ar and H_2O, with one additive pumping photons and the other increasing the O_2 concentration thus facilitating ignition.

The results shown on Figure 3 were fitted with a logarithmic distribution function in order to obtain the ignition probability law (Galton's law); see Eq. 3 and Figure 4.

$$P(E_{inc}, C_1, C_2) = \frac{1}{2} + \frac{1}{2} erf\left[\frac{\ln(\mathrm{E_{inc}}) - C_1}{C_2\sqrt{2}}\right] \quad (3)$$

The same work was carried out by Bane et al. (2011) using a logistic law. Here for the proposed law, C_1 and C_2 are the parameters to be optimized from the experimental data reported in Table 2. From the two parameters we can obtain the mathematical expectation, the mode, and the median (Eq. (4), Eq. (5) and Eq. (6).

$$Expectation = e^{C_1 + 0.5C_2^2} \quad (4)$$

$$Median = e^{C_1} \quad (5)$$

$$\begin{cases} \text{Variance} = \left(e^{C_2^2} - 1\right) e^{2C_1 + C_2^2} \\ \text{Standard deviation} = \sqrt{Variance} \end{cases} \quad (6)$$

Table 2 approximately here

The expected value represents the mean incident energy for the whole dataset. The median is commonly named E_{50}, which is a value corresponding to an ignition probability of 50%. The Table 2 shows statistic parameters about the effect of additives, it can be seen that the configuration with 30 mbar H_2O and 1 % Ar is very interesting the median is 27.11mJ as the lowest incident energy in this case. This law is very effective because for lower incident energies it gives an ignition probability of zero while for other energies the probability is nonzero (Rudz et al., 2014; Bernard et al., 2010).

Figure 4 approximately here

The fitted results on Figure 4 show the ignition law probabilities of the different cases investigated. This facilitates the statistical analysis of the total effect of additive elements. It should be remembered that the effects of both elements (Ar, H_2O) have a very important role in the physics of ignition phenomena, i.e. the plasma physics (creation of a hot spot plasma by focusing laser beams) and the chemical kinetics (development of the flame front) from the n-decane/air mixture.

4.1.2. Influence of Impurities

In this section the quality of the two fuels chosen was tested, i.e., an impure n-decane (94%) and a pure n-decane (99%). Chromatographic analysis and mass spectrometry of a sample of the impure n-decane were performed to investigate the nature of fuel impurities. The results are given in Table 3.

Table 3 approximately here

The ignition frequencies are plotted as a function of incident energy on Figure 5. It can be seen that the laser ignition is very sensitive to the chemical composition of the fuel. Impurities act as an inhibitor at low incident energies (E_{inc}<30 mJ) and as a catalyst at high incident energies (E_{inc}>30 mJ).

Figure 5 approximately here

It is likely that the chemical nature of the 6% of impurities changes the ignition probability because of the behaviour of the other molecules contained in the n-decane fuel (Table 3) located in the focal volume. Certainly this behaviour is related to the different reactivity of these molecules and of the mean free path of each reactive molecule near the ionised atomic elements in the breakdown zone. As reported in Table 3, this influence is due to the 1.6 % of dodecane ($C_{12}H_{26}$) and to the 1% Undecane ($C_{11}H_{24}$): these components have the highest number of carbon atoms and these linear molecules require more energy to be broken.

4.1.3. Influence of the equivalence ratio

Figure 6 presents the probability distributions of ignition tests in pure n-decane (99%)/air mixture as a function of the equivalence ratio. The same kind of statistical study was done with other fuels such as propane (Eckhoff et al., 2010) or hydrogen ethene (Wähner et al., 2013); their work presents similarities with the ignition distributions obtained from electrical spark ignition.

Figure 6 approximately here

The result obtained here is slightly different from the experimental data of Strozzi et al. (2014), where the same mixtures were used in the same conditions but with a different air composition and fuel purity, namely ambient air and impure n-decane (94%).

For rich impure mixtures (94% n-decane+ambient air), Figure 7 shows that the ignition probability decreases far from stoichiometry, whereas in our results, using pure mixtures, ignition frequencies increase with an increase in the equivalence ratio. This result highlights the effect of the impurities contained in the fuel and air used for combustion.

Table 4 approximately here

Table 4 completes the figure 6 by reporting some statistic parameters about the effect of equivalence ratio, the energy E_{50} decreased with the rising of the equivalence ratio, except for Φ = 1.1 however for the stoichiometric state where there was a slightly lower value. An opposite effect was observed with the standard deviation.

When the entire range of incident energies is considered, it was found that stoichiometric and rich mixtures display the best ignitability, whereas with higher incident energies at high ratios (ϕ=1.6 and ϕ=2.0) a decrease in ignitability was observed (see Figure 6). For the leanest mixture (ϕ = 0.65) ignition did not occur with a focal lens of 150 mm. These values were fitted by a logarithmic law for interpolation as a function of incident energy and ignition probability.

The quality of air, impurities and additives contained in the fuel as well as the equivalence ratio affect the ignition probability (see Figure 7). It is clear that regulation of the energy delivered by the laser (incident energy) can be crucial in reaching the systematic ignition regime (probability of ignition $\rightarrow$ 100%).

Figure 7 approximately here

The comparison made in Figure 7 and Table 5 according to a statistical study using Galton's law presents some similarities. For example, at ϕ=0.9 we have approximately

the same standard deviation and for ϕ=2.0 we find approximately the same median. The difference is due to the presence of impurities in the air and fuel.

Table 5 approximately here

Table 5 shows that for ϕ= 0.9 (A), median E_{50} and expected value are close, the same applied for case (C). However, E_{50}(A) is greater than E_{50}(C) but their standard deviation are similar. Mathematically, it means that the curve (C) was almost the curve (A) but translated to the left on the abscissa axis. Physically it was interpreted that the impurities (C) promote the ignition of n-decane uniformly. Concerning ϕ=2.0, the median E_{50} (B) is similar to E_{50} (D), but standard deviation in the (B) case was largely higher than the standard deviation of (D).This result can be interpreted as follow: at high equivalence ratios the impurities have a double effect, it acts like inhibitor at energies lower than E_{50} and as catalyst after, consequently a small zone where ignition probability vary is observed.

4.1.4. Influence of the focal length

The ignition of methane in air was studied by Beduneau et al. (2003) using three focal lengths, 50, 100, 300 mm, to highlight the triple effect of velocity, equivalence ratio and focal length. In this section we highlight the effect of the focal length on the ignition probabilities using two focal lengths (100 and 150 mm). The influence of the latter is reported on Figure 8.

Figure 8 approximately here

The focal effect is quite clear: with a focal length of 150 mm, the ignition zone sometimes begins at 10 mJ and reaches systematic ignition at 80 mJ. With a focal length of 100 mm, the ignition probability begins at E_{inc}>20 mJ and reaches 100% of ignition at E_{inc}=40 mJ. With the shorter focal length, it is possible to ignite the lean

mixture (Φ = 0.65), contrary to the case with a 150 mm focal length. Effects of focal length for different equivalence ratios are reported in Table 6 for the n-decane (99%) / air mixtures.

Table 6 approximately here

For equivalence ratios ranging from 0.9 to 1.6 the shorter focal length (100 mm) the expected values, medians and standard deviations drastically dropped. It also seems that the E_{50} tends to a limit about 25 mJ. Moreover, contrary to the case with the focal length of 150 mm, it was possible to ignite the leanest mixture Φ = 0.65. The focal effect can be explained with the existing link between the focal length and the resulting intensity of the laser beam at the waist (the focal point), see Figure 9 and Eq. (7) to (9).

Figure 9 approximately here

$$\begin{cases} r = \left(\frac{2\lambda}{\pi}\right)\left(\frac{f}{d}\right) \\ l = \left(\sqrt{2}-1\right)\frac{\theta}{d} f^2 \end{cases} \qquad (7)$$

r is the waist, *l* is the spot size length, *f* represents the focal length (100 and 150 mm), λ is the laser wavelength (1064 nm), *d* is the beam diameter (6 mm), and θ is the beam divergence (0.3962 mrad). The pulse duration (t_{pulse}) is 4.48 ns. We assume that the focal point is like a cylinder, then:

$$Focal\ volume = \pi r^2 l \qquad (8)$$

The physical characteristic of the power energy and the power density energy at the focal point related to the geometric feature are given by Eq. 9.

$$\begin{cases} Power = \left(\dfrac{E_{laser}}{t_{pulse}} \right) \\ Focal\ density\ power = \left(\dfrac{Power}{\pi\, r^2} \right) \end{cases} \tag{9}$$

Figure 10 approximately here

This influence can be explained by the high power density of the laser at the focal volume which is inversely proportional to the focused hot spot plasma waist, as shown in Figure 10. Note that when the focal length is short, the focal volume will also be lower (see Table 7) with a high intensity power. The focal properties can be found in Maxim Thys (2011).

Table 7 approximately here

Hydrodynamic phenomena (Cardin et al., 2013a; Griffiths et al., 2015b) and thermal effects (Catoire & Naudet, 2005) have also to be taken into account for a complete characterisation of this ignition system.

4.2. Minimum Ignition Energy

In order to compare our results to the data of Strozzi et al. (2014), *MIE* measurements are summed up in Figure 11, using the approach developed in Moorhouse et al. (1974) .

Figure 11 approximately here

The first point to note is that the curve obtained has the typical U-shape. In Strozzi et al. (2014) the authors worked with the same pressure and temperature

conditions and with a comparable range of incident energies and equivalence ratios; however, the purity of n-decane was only *94 %* and was mixed with ambient air.

It can be clearly seen that for lean mixtures the impure n-decane needs to absorb less energy to ignite whereas for rich mixtures the behavior is the reverse. Moreover, as in Strozzi et al. (2014), the studied mixture was not ignited for the leanest equivalence ratio. One can note that this equivalent ratio ($\Phi = 0.65$) is close to the Lower Flammability Limit ($\Phi = 0.55$) calculated using the experimental correlation given in (Catoire & Naudet, 2005).

4.3. Ignition Delay Time (IDT)

4.3.1. Global Ignition Delay Time (GIDT) measurements by fast photodiode

The G*IDT* parameter was first measured with a fast infrared detector and all the results were approximated using an Arrhenius-based law for each equivalence ratio as a function of the absorbed energy (see Figure 12).

Figure 12 approximately here

The dispersion of this parameter is a function of the equivalence ratio (Φ): a short ignition delay time and low dispersion were recorded near stoichiometry ($\Phi = 1.1;\ 13.43 < \tau\ (ms) < 20.12$), whereas far from this operating point, the inverse effect was observed, e.g. ($\Phi = 2;\ 30.9 < t\ (ms) < 61.78$) (see Figure 12). This wide dispersion is due to the different ignition modes. With a high concentration of oxygen (lean mixtures), there is a greater probability of ionizing molecules of oxygen than molecules of $C_{10}H_{22}$, resulting in the production of OH^* and formaldehyde CH_2O, as ignition requires more time to produce a sufficient amount of electron avalanches and ions to start the combustion.

With a high concentration of n-decane, there is a greater probability of creating radicals of CI^*, CII^* and CH^* which initiate and maintain the chemical chain reactions.

But at stoichiometry, there is a balanced creation of different radical fractions which provides an almost perfect balance to quickly initiate and maintain ignition. The mathematical law which we developed from the experimental data to retrieve the ignition delay time as a function of the absorbed energy is given by Eq. 10. The experimental values of the parameters (*A*) and (*B*) are given in Table 8.

$$t_{ind}(ms) = A\exp\left[\frac{B}{E_{abs}}\right] \qquad (10)$$

Table 8 approximately here

All the values of (*A*) and (*B*) were calculated at atmospheric pressure and an initial temperature of (*347 K*).

4.3.2. Chemical Ignition Delay Time (CIGT) measurements by light emission spectroscopy

This optical apparatus allows measuring the CIGT from which a radical radiation or a chemical species related to a fixed wavelength appears. As shown in Figure 13, the CIGT was estimated from the spectroscopic measurements which represent one case of laser breakdown ignition and the flame emission spectroscopy as a function of time. Integration time of one spectrum was about *2 ms*.

Figure 13 approximately here

On the complete spectrum, the bands emitted during the breakdown from *0 ms* to about *2.5 ms* can be observed (Figure 13). The laser beam light emission is clearly visible at *1064 nm* and indicates the start of the process. The relaxation of ionized states of nitrogen, oxygen and carbon *NI, NII, OII, OIII* and *CI…* generates the free radicals OH^*, CH^* and CII^*, which can be distinguished just after breakdown by the low intensity emission line. See the Figure 14 which represents the breakdown spectrum of the ionized atomic states and the flame spectrum emission of some detected species and some free radicals.

Figure 14 approximately here

These spectra make it possible to carry out analyses of the different Chemical Delay Times represented by a fixed emission wavelength of four radicals CII^*, OH^*, CH^*, CI^*. The procedure is to follow a specific wavelength in time, taking its tangent between (*20%* and *80%)* of the maximum signal strength and making it cut the time-axis. The spark is indicated by the peak of the *1064 nm* laser beam. Lastly, the estimated chemical delay is the difference between the time recorded by the intersection of the tangent line with the time-axis and the first appearance of the focused laser beam, as indicated on the figure.13 for the OH^* radical.

Figure 15 approximately here

Variations in the corresponding ignition delay as a function of the equivalence ratio are plotted in Figure 15. For lean mixtures, the OH^* radical is the first to appear, followed by the CH^* radical and then CII^* and CI^*. The lowest chemical induction delay is recorded for CII^*near stoichiometry and is about *11.74 ms* with minor error dispersion.

The observations from these results can be a significant help in developing correct kinetic schemes. They should also improve numerical simulations to obtain the actual induction time in the same experimental conditions (Laser ignition).

5. Conclusion

The present experimental investigation completes many studies on laser ignition of different fuels in the monophasic (gas) or biphasic (gas liquid) state, for example Alcohols, Alkanes , Ethers, multi-component fuel (jet A, JP8...). Previous studies have shown that ignition behaviours are strongly dependent on the fuel considered. One important conclusion of this study concerns the effect of Argon and Moisture. The configuration with 30 mbar H_2O and 1 % Ar acts as a catalyst on the ignition of the n-decane/air mixture. The comparison between the two n-decanes investigated shows that hydrocarbon impurities can change the behaviour of the fuel during ignition. The effect of the equivalence ratio has also been highlighted in the case of pure n-decane and we have compared our results with the ignition data of Strozzi et al., 2014 with 6% impurities and ambient air. The effect of impurities is favourable for ignition in the case of lean mixtures whereas pure decane is easier to ignite for rich mixtures.

The focal length is another effect which we have studied and our results show that a short focal length increases the ignition probabilities because of the resulting short focal volume. In the case of the 100 mm focal length, an intense rise in the ignition probability is recorded; the operating range for the two focal lengths differs as a function of the incident energy: between 20 to 40 mJ for 100 mm and between 10 to 60 mJ for the 150 mm focal length.

In the second part of this experimental study, the Minimum Ignition Energy (*MIE*) and the Ignition Delay Time (*IDT*), at fixed atmospheric pressure and temperature, were measured for six equivalence ratios, in the case of pure 99.9% n-decane. *MIE* was determined for this pure n-decane, and compared with the data of Strozzi et al. (2014) for impure n-decane. This comparison highlights the influence of impurities on laser induced ignition.

It was shown that impurities act as a catalyst for ignition at lower ratios and as an inhibitor for higher ratios. It is noticeable that a small amount of impurities (about *6 %*) can play a significant role in the ignition characteristics. The study next focused on measuring the Ignition Delay Time with a fast infra-red detector. We proposed an Arrhenius-based law which gives the variation of this parameter as a function of the equivalence ratio and absorbed energy. This work showed that the dispersion of the *IDT* increases at lower and higher equivalence ratios and is minimum near stoichiometry (ϕ*=1.1*). We also demonstrated the effect of the absorbed energy on the *IDT*: for low absorbed energies, the ignition time tends to infinity and for considerable energy absorbed the ignition time tends to a limit which is a function of the stoichiometry. By spectroscopic measurements, the different chemical Induction Delay Times were monitored for 4 radicals (CII^*, OH^*, CH^*, CI^*). This provides a validation of the initial results achieved with the IR detector because the same influence of the equivalent ratio was recorded. This study is part of a broader research program that plans investigations on the influence of the addition of argon and moisture on ignition conditions (Gillard et al., 2014.). The next step in this study will be to conduct tests on dodecane alone or mixed with n-decane. The pyrolysis products of these two surrogates could also be taken into account with the same conditions of pressure and temperature on ignition properties as those used in this paper.

Acknowledgements

The author gratefully acknowledges the financial contribution of Région Centre Val de Loire, the Labex Caprysses of Orleans University and French CNRS.

References

Bane, S. P. M., Shepherd, J. E., Kwon, E., & Day, a. C. (2011). Statistical analysis of electrostatic spark ignition of lean H2/O2/Ar mixtures. *International Journal of Hydrogen Energy*, *36*(3), 2344–2350. doi:10.1016/j.ijhydene.2010.05.082

Beduneau, J. (2003). Measurements of minimum ignition energy in premixed laminar methane/air flow by using laser induced spark. *Combustion and Flame*, *132*(4), 653–665. doi:10.1016/S0010-2180(02)00536-9

Bernard, S., Lebecki, K., Gillard, P., Youinou, L., & Baudry, G. (2010). Statistical method for the determination of the ignition energy of dust cloud-experimental validation. *Journal of Loss Prevention in the Process Industries*, *23*(3), 404–411. doi:10.1016/j.jlp.2010.01.006

Boretti, A. (2013). Water injection in directly injected turbocharged spark ignition engines. *Applied Thermal Engineering*, *52*(1), 62–68. doi:10.1016/j.applthermaleng.2012.11.016

Cardin, C., Renou, B., Cabot, G., & Boukhalfa, A. (2013a). Experimental analysis of laser-induced spark ignition of lean turbulent premixed flames. *Comptes Rendus Mécanique*, *341*(1-2), 191–200. doi:10.1016/j.crme.2012.10.019

Cardin, C., Renou, B., Cabot, G., & Boukhalfa, A. M. (2013b). Experimental analysis of laser-induced spark ignition of lean turbulent premixed flames: New insight into ignition transition. *Combustion and Flame*, *160*(8), 1414–1427. doi:10.1016/j.combustflame.2013.02.026

Catoire, L., & Naudet, V. (2005). Estimation of temperature-dependent lower flammability limit of pure organic compounds in air at atmospheric pressure. *Process Safety Progress*, *24*(2), 130–137. doi:10.1002/prs.10072

Chehroudi, B. (2004). Laser Ignition For Combustion Engines.

Eckhoff, R. K., Ngo, M., & Olsen, W. (2010). On the minimum ignition energy (MIE) for propane/air. *Journal of Hazardous Materials*, *175*(1-3), 293–7. doi:10.1016/j.jhazmat.2009.09.162

Gillard, P., Mokrani, N., Rudz, S., Strozzi, C., & Tihay, V. (n.d.). Effect of moisture and argon on laser ignition of ethanol and decane. *X ISHPMIE Tenth International Symposium Bergen, Norway 10-14 June 2014*, (Hazards, Prevention, and Mitigation of industrial Explosions), 11.

Griffiths, J., Riley, M. J. W., Borman, a., Dowding, C., Kirk, a., & Bickerton, R. (2015a). Effect of flow velocity and temperature on ignition characteristics in laser ignition of natural gas and air mixtures. *Optics and Lasers in Engineering*, *66*, 132–137. doi:10.1016/j.optlaseng.2014.09.002

Griffiths, J., Riley, M. J. W., Borman, a., Dowding, C., Kirk, a., & Bickerton, R. (2015b). Effect of flow velocity and temperature on ignition characteristics in laser ignition of natural gas and air mixtures. *Optics and Lasers in Engineering*, *66*, 132–137. doi:10.1016/j.optlaseng.2014.09.002

Hatwar, P., & Verma, D. (2012). Laser Ignition in Internal Combustion Engines, *2*(2), 341–345.

He, Z., Jing, Q., Zhu, L., Zhang, W., & Huang, Z. (2015). The effects of different intake charge diluents on the combustion and emission characteristics of a spark ignition natural gas engine. *Applied Thermal Engineering*, *89*(x), 958–967. doi:10.1016/j.applthermaleng.2015.06.072

Jain, V., & Kozola, S. (2001). Measurements of Minimum Ignition Energy By Using Laser Sparks for Hydrocarbon Fuels in Air : Propane , Dodecane , and Jet-A Fuel, *1328*, 1320–1328.

Jiping, L., Keqiang, C., Xiaobo, Z., Jinshi, W., Junjie, Y., & Deguchi, Y. (2015). Numerical Simulation on the Laser Induced Oxygen Spark under Different Ambient Conditions. *Energy Procedia*, *75*, 2409–2414. doi:10.1016/j.egypro.2015.07.194

Jones, R. E. (1978). Gas turbine engine emissions-Problems, progress and future. *Progress in Energy and Combustion Science*, *4*(2), 73–113. doi:10.1016/0360-1285(78)90006-0

Karthikeya Sharma, T. (2014). Performance and emission characteristics of the thermal barrier coated SI engine by adding argon inert gas to intake mixture. *Journal of Advanced Research*, (2). doi:10.1016/j.jare.2014.06.005

Li, W., Liu, Z., Wang, Z., & Dou, H. (2015). Experimental and theoretical analysis of effects of atomic, diatomic and polyatomic inert gases in air and EGR on mixture properties, combustion, thermal efficiency and NOx emissions of a pilot-ignited NG engine. *Energy Conversion and Management*, *105*, 1082–1095. doi:10.1016/j.enconman.2015.08.052

Lilley, D. G. (2003). *High temperature Air Combustion*. (Ashwani K. Gupta, Ed.) (High tempe.). Björn Karlsson and James G. Quintiere.

Maxim Thys, E. D. (2011). *Laser Beams: Theory, Properties & Applications*. *New York*.

McNeill, D. H. (2005). Minimum ignition energy for laser spark ignition. *Proceedings of the Combustion Institute*, *30*(2), 2913–2920. doi:10.1016/j.proci.2004.07.026

Mokrani, N., Rudz, S., & Gillard, P. (2015). Influence de l'argon sur la durée de relaxation du plasma induit par claquage laser. *CAE XII. Arc Électrique et Plasma Thermique*, (1), 6.

Moorhouse, J., Williams, A., & Maddison, T. E. (1974). An investigation of the minimum ignition energies of some C1 to C7 hydrocarbons. *Combustion and Flame*, 203–213.

Morsy, M. H., & Chung, S. H. (2002). Numerical simulation of front lobe formation in laser-induced spark ignition of ch 4 /air mixtures, *29*, 1613–1619.

Nikolaou, Z. M., Chen, J. Y., & Swaminathan, N. (2013). A 5-step reduced mechanism for combustion of CO/H2/H2O/CH4/CO2 mixtures with low hydrogen/methane and high H2O content. *Combustion and Flame*, *160*(1), 56–75. doi:10.1016/j.combustflame.2012.09.010

Pakter, R. (1998). Intensity effects on inverse-bremsstrahlung electron acceleration. *Physical Review E*, *58*(2), 2501–2504. doi:10.1103/PhysRevE.58.2501

Phuoc, T. X. (2006). Laser-induced spark ignition fundamental and applications. *Optics and Lasers in Engineering*, *44*(5), 351–397. doi:10.1016/j.optlaseng.2005.03.008

Rudz, S., Chetehouna, K., Strozzi, C., & Gillard, P. (2014). Minimum Ignition Energy Measurements for α-Pinene/Air Mixtures. *Combustion Science and Technology*, *186*(10-11), 1597–1605. doi:10.1080/00102202.2014.935604

Starikovskiy, A., & Aleksandrov, N. (2013). Plasma-assisted ignition and combustion. *Progress in Energy and Combustion Science*, *39*(1), 61–110. doi:10.1016/j.pecs.2012.05.003

Strozzi, C., Gillard, P., & Minard, J.-P. (2014). Laser-Induced Spark Ignition of Gaseous and Quiescent N-Decane–Air Mixtures. *Combustion Science and Technology*, *186*(10-11), 1562–1581. doi:10.1080/00102202.2014.935601

Thiele, M., Selle, S., Riedel, U., Warnatz, J., & Maas, U. (2000). Numerical simulation of spark ignition including ionization. *Proceedings of the Combustion Institute*, *28*(1), 1177–1185. doi:10.1016/S0082-0784(00)80328-8

Tihay, V., Gillard, P., & Blanc, D. (2012). Ignition study of acetone/air mixtures by using laser-induced spark. *Journal of Hazardous Materials*, *209-210*, 372–8. doi:10.1016/j.jhazmat.2012.01.040

Tran X. Phuoc. (1999). Laser-Induced Spark Ignition of CH 4 / Air Mixtures, *2180*(99), 203–216.

Wähner, A., Gramse, G., Langer, T., & Beyer, M. (2013). Determination of the minimum ignition energy on the basis of a statistical approach. *Journal of Loss Prevention in the Process Industries*, *26*(6), 1655–1660. doi:10.1016/j.jlp.2013.06.002

Zhang, B., Shen, X., & Pang, L. (2015). Effects of argon/nitrogen dilution on explosion and combustion characteristics of dimethyl ether–air mixtures. *Fuel, 159*, 646–652. doi:10.1016/j.fuel.2015.07.019

List of Figures

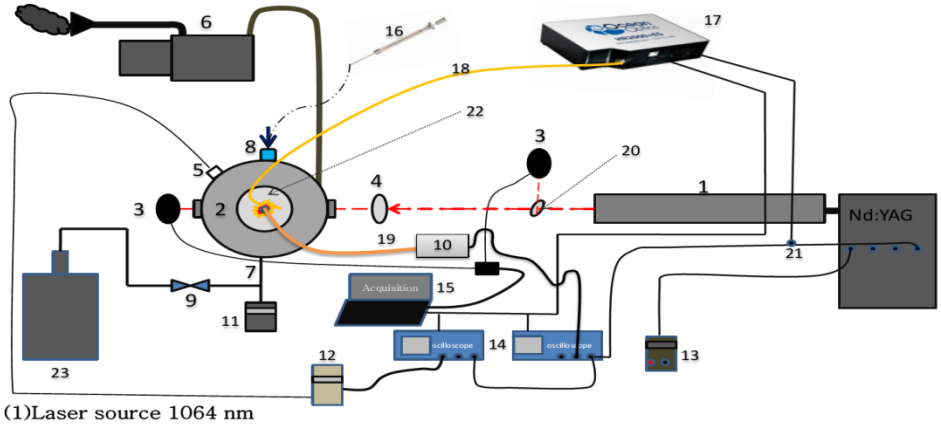

(1)Laser source 1064 nm
(2)Combustion chamber
(3)Ophir Nova energy meter
(4)Focal lens
(5)Pressure sensor
(6)Vacuum pump
(7): Gas inlet
(8): Symptum
(9)Valve
(10)Infrared detector
(11)Pressure gauge
(12)Amplifier
(13)Laser controller
(14)Oscilloscopes
(15)Acquisition unit
(16)Syringe
(17)HR 2000+ ES Spectrometer
(18)(19)Optical fibers
(20)Beam-splitter
(21)Laser trigger command
(22)Quartz orthogonal window
(23) Pure air (N_2O_2)

Figure 1. Schematic diagram of the apparatus used.

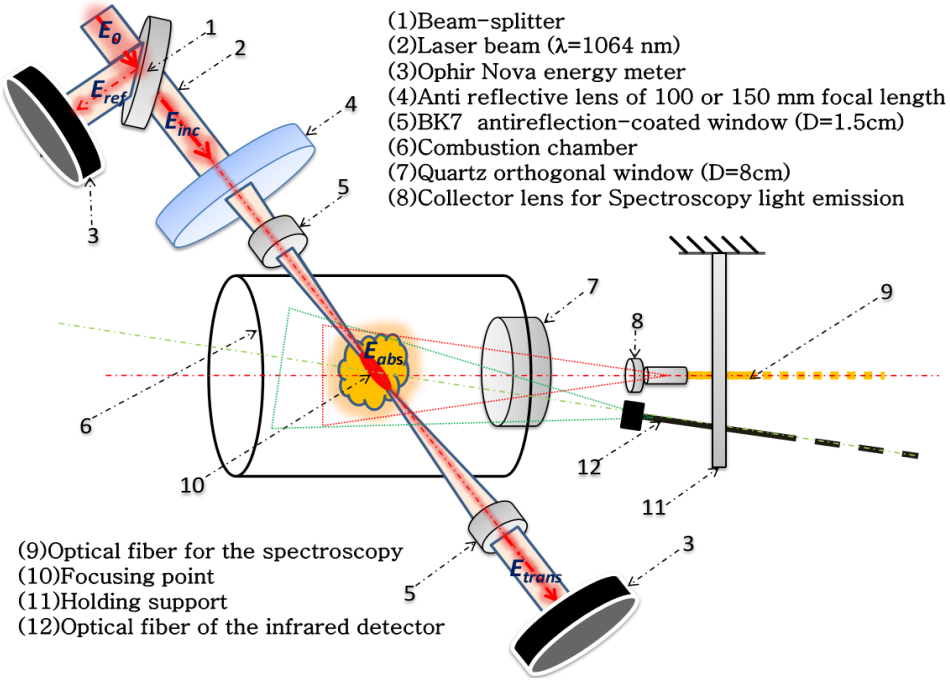

(1)Beam-splitter
(2)Laser beam (λ=1064 nm)
(3)Ophir Nova energy meter
(4)Anti reflective lens of 100 or 150 mm focal length
(5)BK7 antireflection-coated window (D=1.5cm)
(6)Combustion chamber
(7)Quartz orthogonal window (D=8cm)
(8)Collector lens for Spectroscopy light emission
(9)Optical fiber for the spectroscopy
(10)Focusing point
(11)Holding support
(12)Optical fiber of the infrared detector

Figure 2. Arrangement of measuring instruments and the principle of operation.

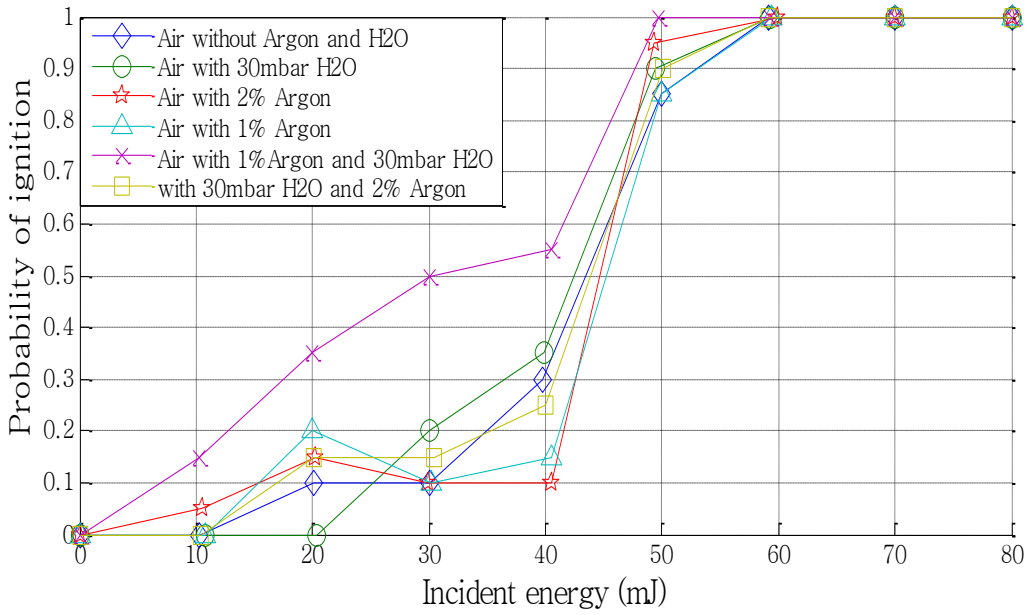

Figure 3. Influence of Argon and moisture on the real ignition frequencies of decane (94% of purity and focal length =150mm) for Φ =1.1

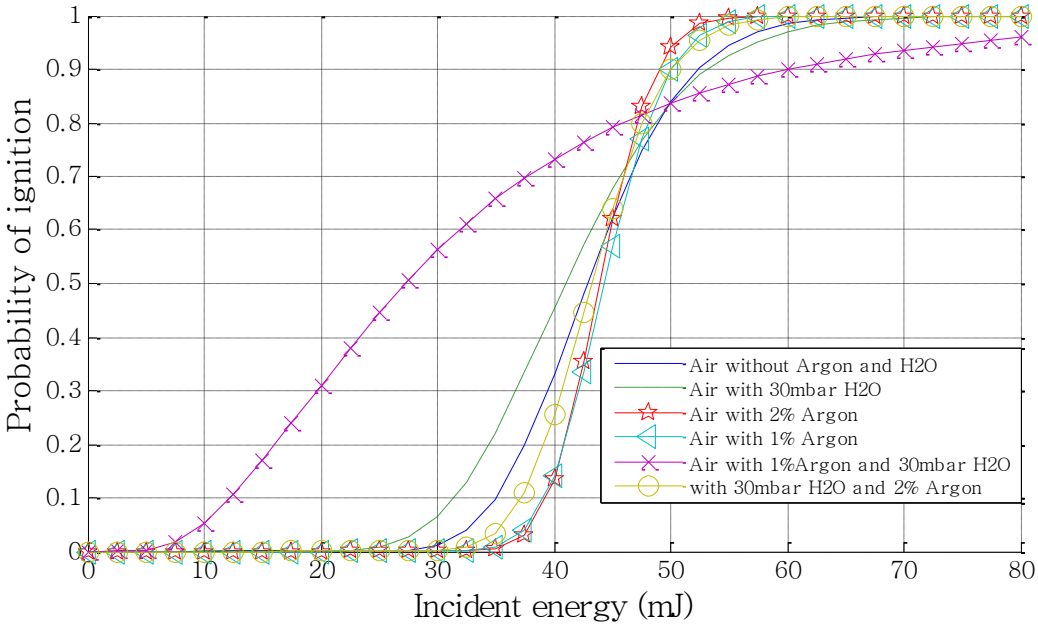

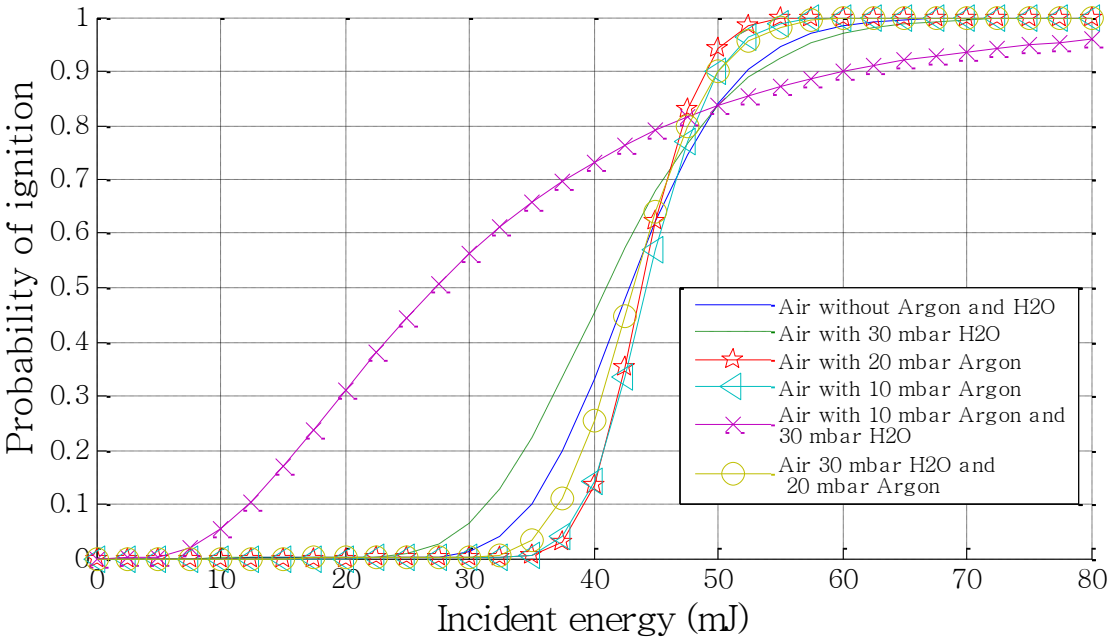

Figure 4. Ignition probability distribution developed from the experimental data.

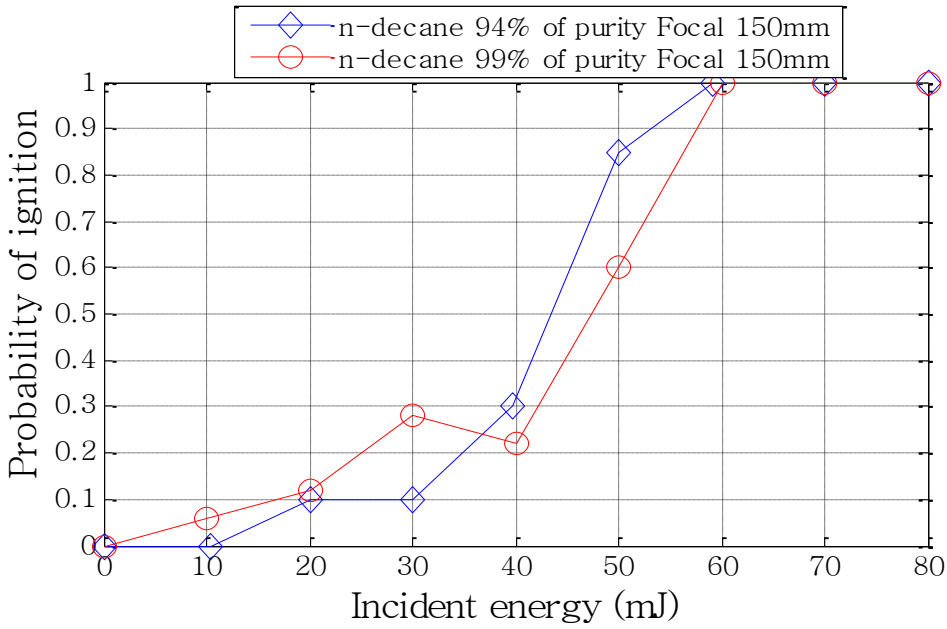

Figure 5. Ignition probability of pure and impure n-decane(ϕ=1.1).

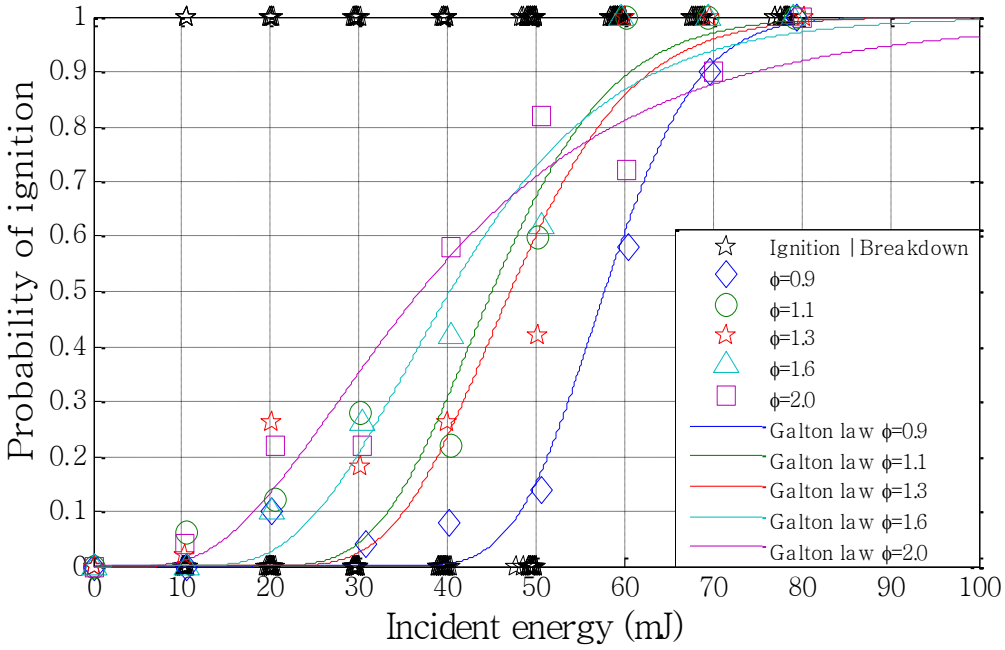

Figure 6. Influence of the equivalence ratio on the ignition frequencies (Pure n-decane 99% and focal length =150mm).

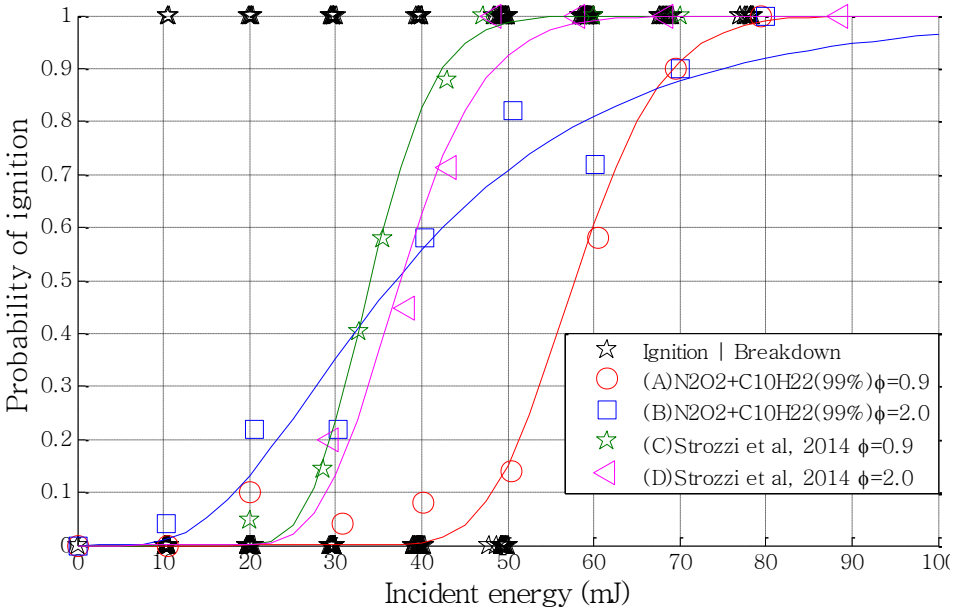

Figure 7. Influence of the equivalence ratio impurities and the used air for combustion (focal length =150mm).

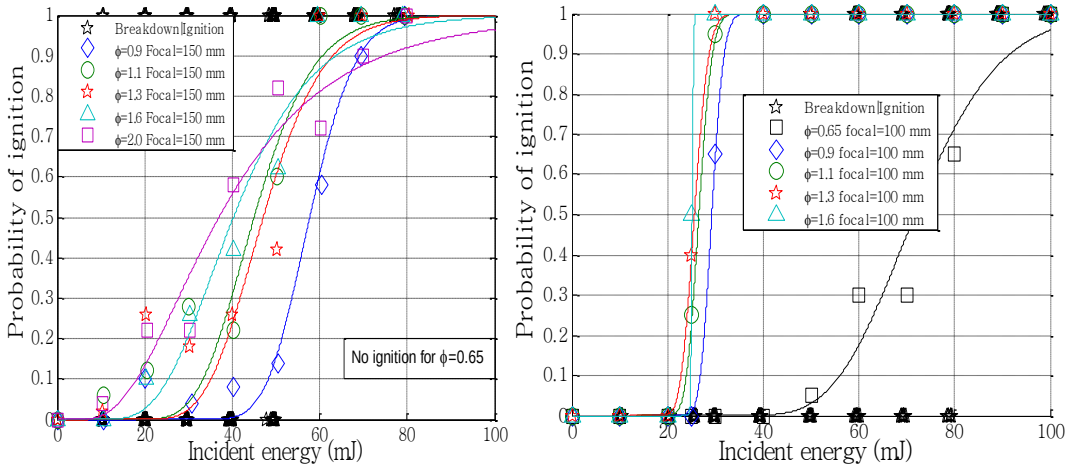

Figure 8. Influence of the focal length (Pure n-decane 99%).

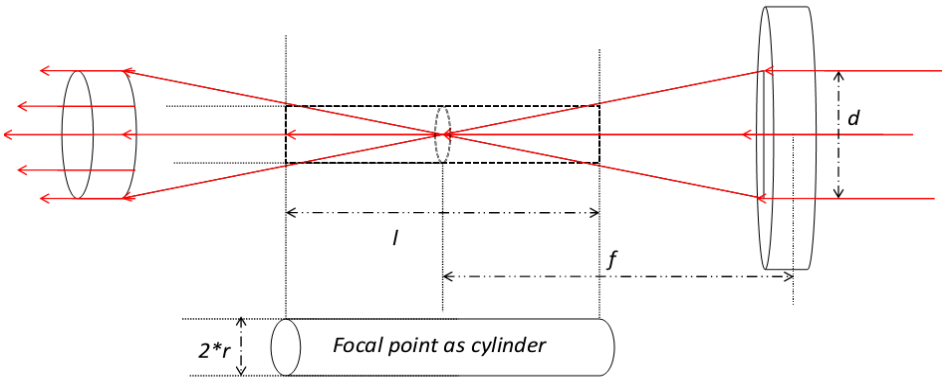

Figure 9. The Geometric characteristics of the focal points

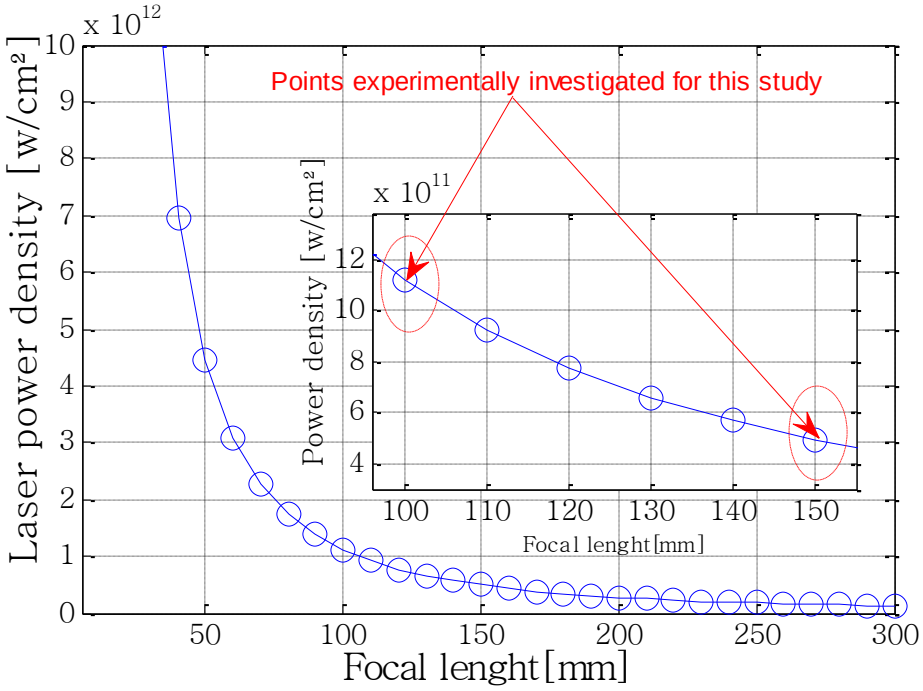

Figure 10. Focal laser power density for E_{laser}=20 mJ.

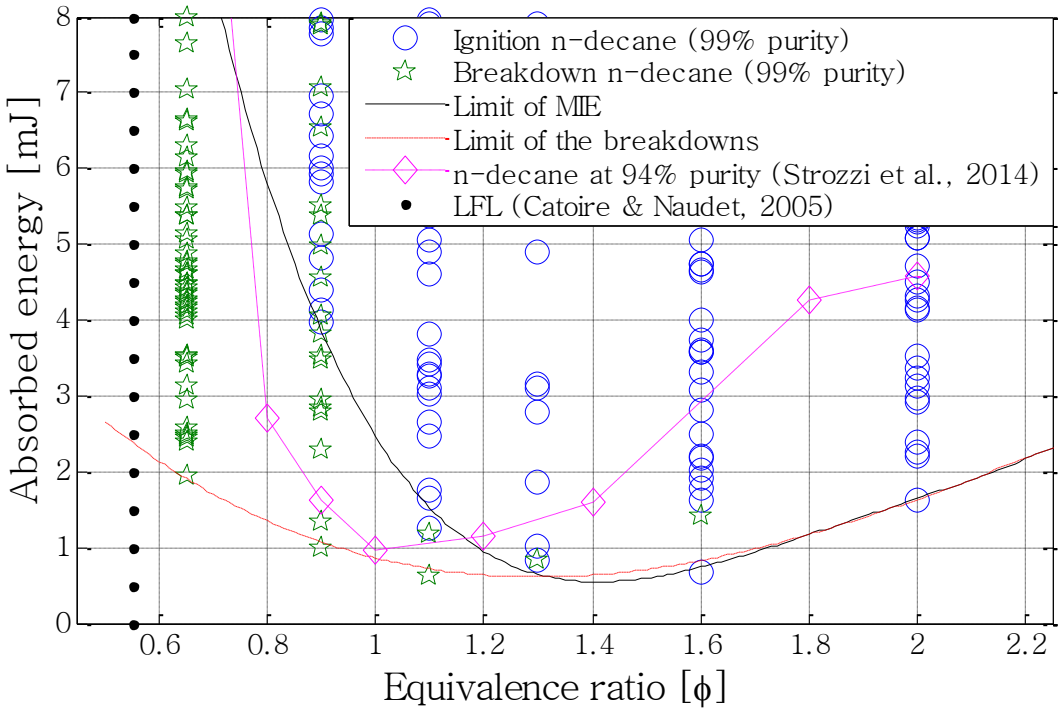

Figure 11. Influence of equivalence ratio (Pure n-decane 99%, focal =150mm)

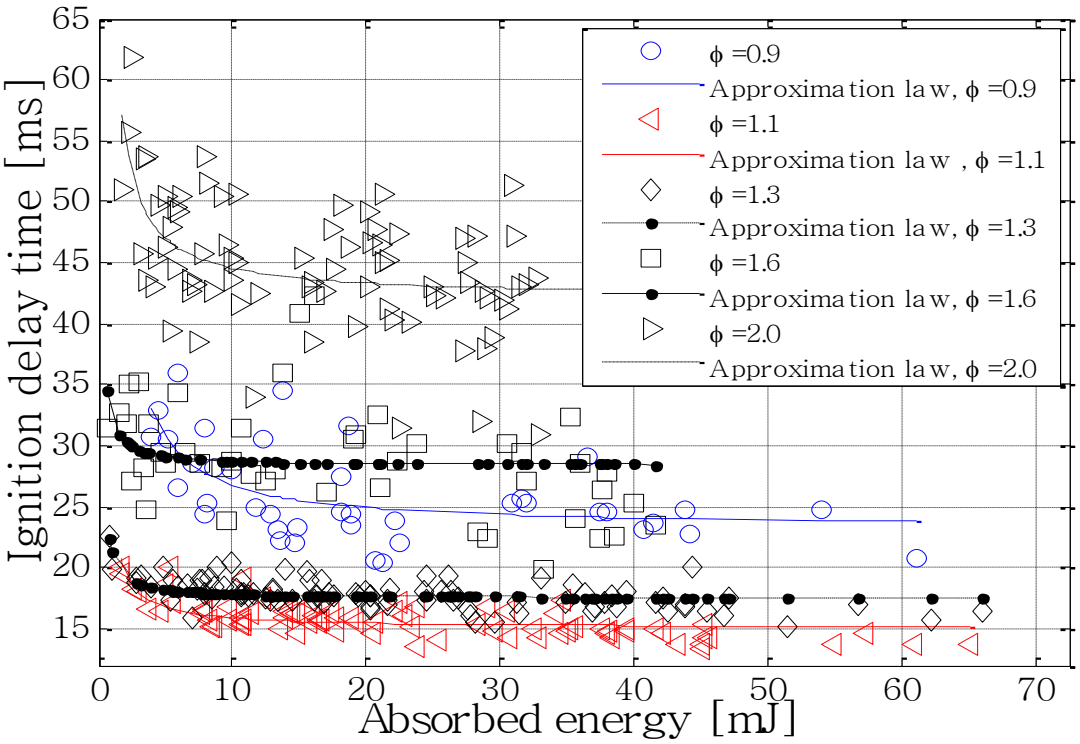

Figure 12. Influence of deposited energy (Pure n-decane 99% and focal = 150 mm)

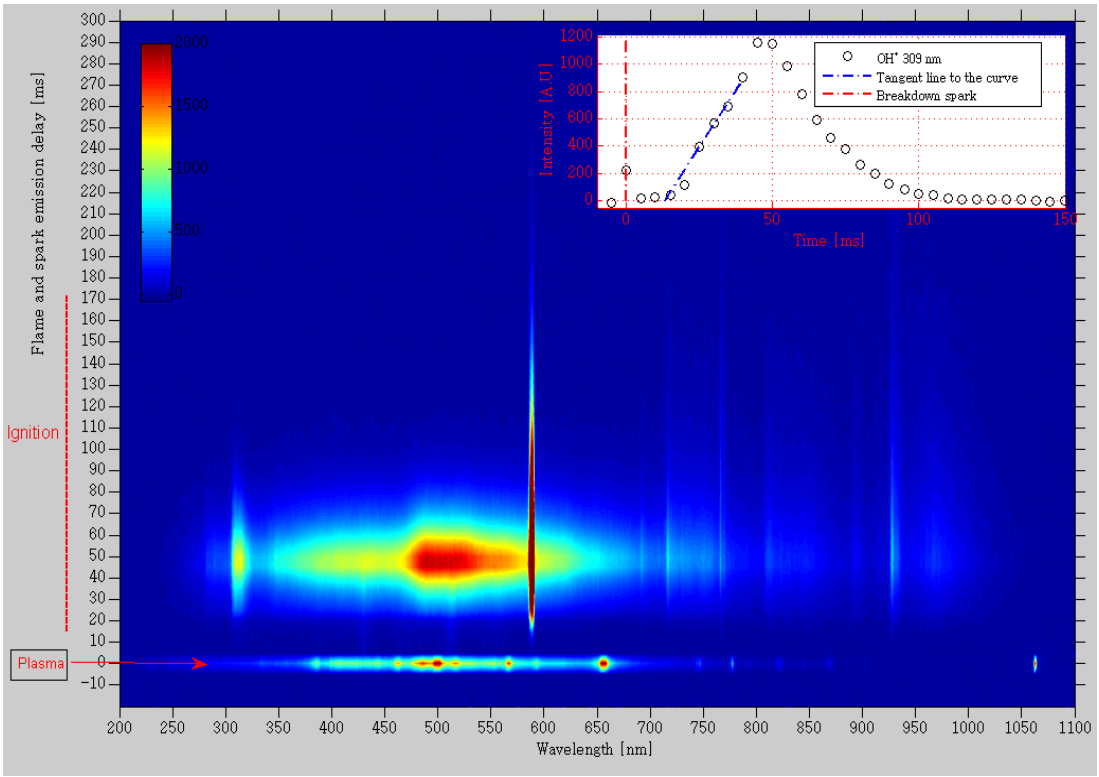

Figure 13. Laser spark ignition and flame emission delay time using spectroscopy

(ϕ = 1.1; E_{inc} = 60mJ).

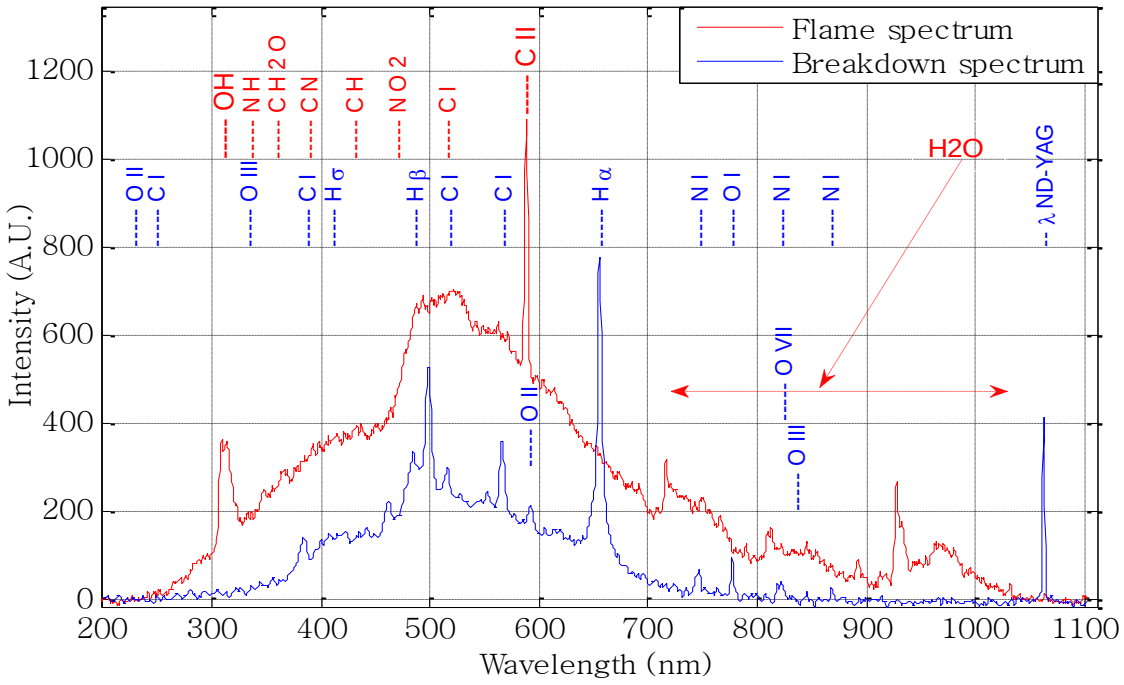

Figure 14. Breakdown ignition and flame emission spectrums (ϕ = 1.1; E_{inc} = 60mJ).

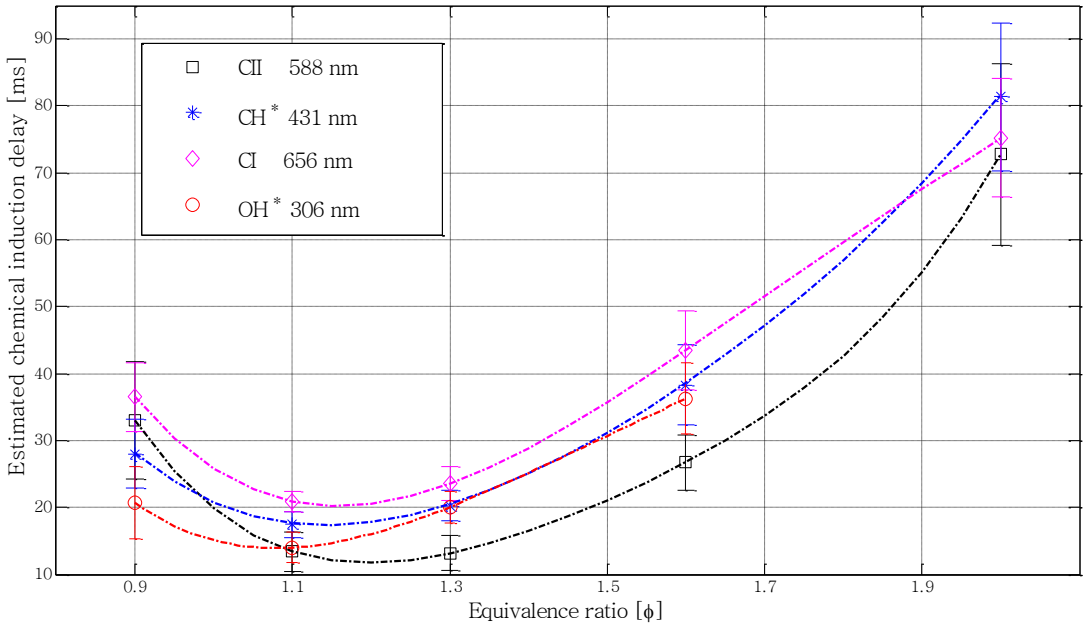

Figure 15. Estimated chemical induction delay as a function of equivalence ratio.

List of Tables

Table 1. Experimental design for the first study.

Argon [%] / H_2O [mbar]	0 [%]	1.0 [%]	2.0 [%]
0	120 shots	120 shots	120 shots
15	120 shots	120 shots	120 shots
30	120 shots	120 shots	120 shots

Table 2. Parameters C_1 and C_2 of the stochastic law.

Parameters / $C_{10}H_{22}$+Composition	C_1	C_2	Expectation value [mJ]	Standard deviation [mJ]	Median (E_{50}) [mJ]
N_2+O_2	3.75	0.15	43.00	6.49	42.52
N_2+O_2+30mbar H2O	3.71	0.20	41.68	8.42	40.85
N_2+O_2+2% Ar	3.78	0.08	43.96	3.52	43.82
N_2+O_2+1% Ar	3.79	0.09	44.44	4.01	44.26
N2+O2+30mbar H2O+1% Ar	3.30	0.62	33.73	23.55	27.66
N_2+O_2+30mbar H2O+2% Ar	3.76	0.11	43.21	4.77	42.95

Table 3. Nature of impurities contained in n-decane (94%).

Time (min)	Compound	Molecule	Percentage
5	Nonane	C_9H_{20}	0.5 **%**
5.5	Nonene	$CH_3(CH_2)_6CH=CH_2$	0.6 **%**
6.5	Decane	$C_{10}H_{22}$	94 **%**
8.1	Undecane	$C_{11}H_{24}$	1.0 **%**
8.6	Undecene	$CH_3(CH_2)_8CH=CH_2$	Unknown **%**
9.6	Dodecane	$C_{12}H_{26}$	1.6 **%**

Table 4. Stochastic law parameters effect of equivalence ratio.

Parameters / ϕ	C_1	C_2	Expectation Value [mJ]	Median E_{50} [mJ]	Standard Deviation (σ)[mJ]
0.9	4.06	0.14	58.33	57.75	8.23
1.1	3.81	0.23	46.26	45.01	10.99
1.3	3.85	0.23	48.34	47.10	11.19
1.6	3.70	0.36	42.96	40.27	15.97
2.0	3.61	0.55	43.03	36.96	25.64

Table 5. Parameters C_1 and C2 of stochastic law effect of impurities.

Parameters / Composition of	Φ	C_1	C_2	Expectation value [mJ]	Standard Deviation (σ) [mJ]	Median E_{50} [mJ]
(A): N_2O_2+$C_{10}H_{22}$(99%)	***0.9***	4.05	0.14	58.3	8.23	57.8
(B): N_2O_2+$C_{10}H_{22}$(99%)	***2.0***	3.60	0.55	43.0	25.64	37.0
(C): Strozzi et al 2014	***0.9***	3.52	0.17	34.5	6.00	34.0
(D): Strozzi et al 2014	***2.0***	3.62	0.20	38.3	7.72	37.5

Table 6. Stochastic law parameters, effect of the focal length.

Focal length [mm]	100			150		
Parameters / ϕ	Expectation Value [mJ]	Median E_{50} [mJ]	standard deviation [mJ]	Expectation Value [mJ]	Median E_{50} [mJ]	Standard deviation [mJ]
0.65	73.07	71.74	14.15	No ignition		
0.9	29.32	29.25	1.97	58.33	57.75	8.23
1.1	26.63	26.55	2.15	46.26	45.01	10.99
1.3	25.71	25.60	2.31	48.34	47.10	11.19
1.6	25.14	25.14	0.50	42.96	40.27	15.97
2.0	No experiment			43.03	36.96	25.64

Table 7. Geometric characteristics of focal points.

Focal length [mm]	**length[μm]**	**Radius[μm]**	**Focal Volume [m^3]**	**Power intensity for $_{E=20mJ}$[W/m^2]**
150	615.41	16.93	$5.54\ 10^{-13}$	$4.955\ 10^{11}$
100	273.51	11.28	$1.09\ 10^{-13}$	$11.15\ 10^{11}$

Table 8. Experimental values of (A) and (B).

Parameters / ϕ	**A**	**B**
0.9	*23.24*	*1.400*
1.1	*15.04*	*0.539*
1.3	*17.49*	*0.203*
1.6	*28.36*	*0.133*
2.0	*42.16*	*0.546*